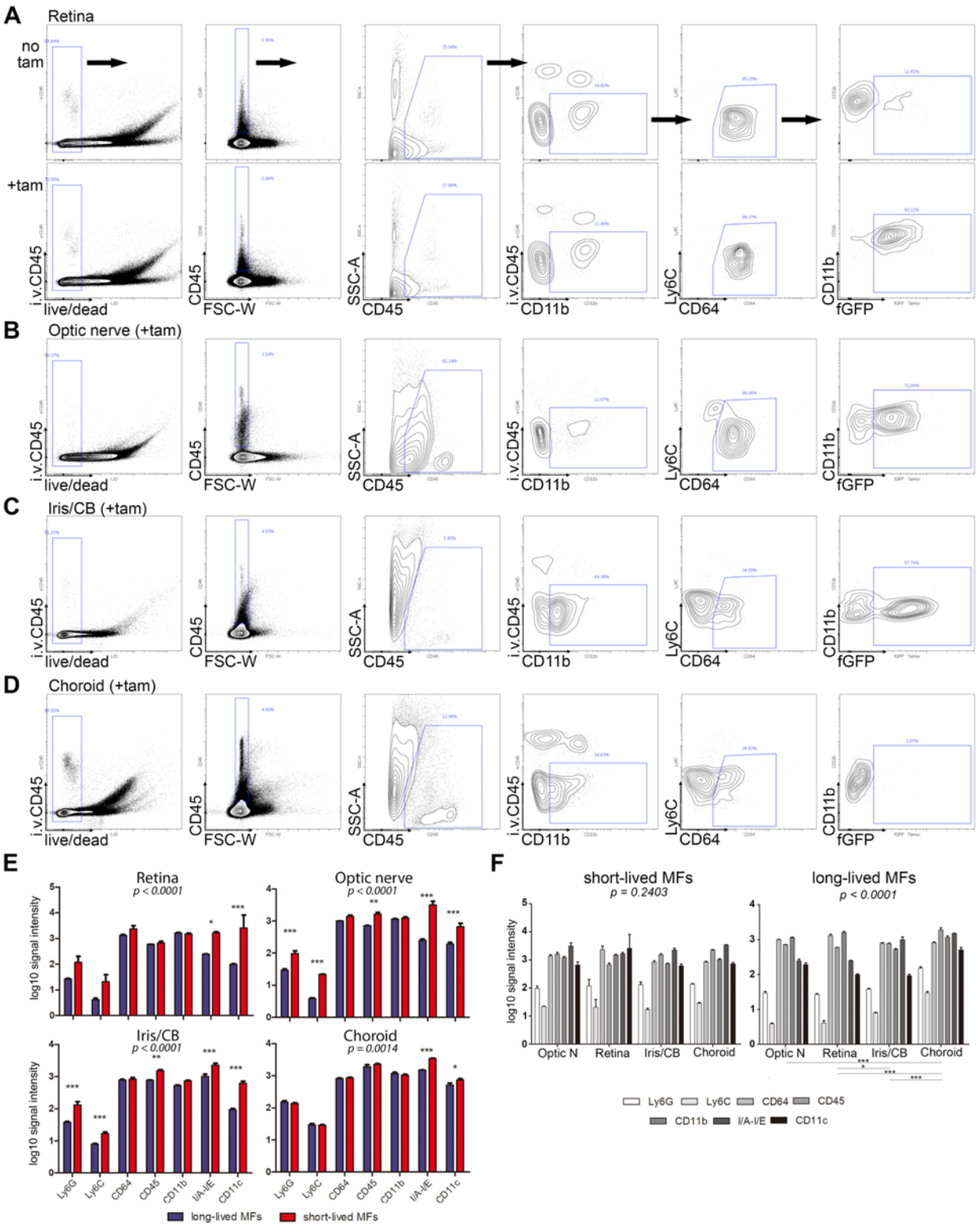
A
Retina
no tam
+tam
i.v.CD45
live/dead
CD45
FSC-W
SSC-A
CD45
i.v.CD45
CD11b
Ly6C
CD64
CD11b
fGFP
B
Optic nerve (+tam)
C
Iris/CB (+tam)
D
Choroid (+tam)
E
Retina
p < 0.0001
Optic nerve
p < 0.0001
Iris/CB
p < 0.0001
Choroid
p = 0.0014
log10 signal intensity
Ly6G
Ly6C
CD64
CD45
CD11b
I/A-I/E
CD11c
long-lived MFs
short-lived MFs
F
short-lived MFs
p = 0.2403
long-lived MFs
p < 0.0001
log10 signal intensity
Optic N
Retina
Iris/CB
Choroid
Ly6G
Ly6C
CD64
CD45
CD11b
I/A-I/E
CD11c

Figure S1. Comparisons of macrophages across different anatomic structures of the eye, Related to Figure 1. (A-D) Representative gating strategies of macrophages in retina (A), optic nerve (B), iris/ciliary body (C) and choroid (D). (B-D) Tissues only shown from tam-pulsed mice. Note, i.v. CD45 indicates i.v. injected CD45 antibody prior to euthanasia to label intravascular cells. **(E, F)** Bar graphs (mean ± SEM) compare long-lived and short-lived macrophages in the retina, optic nerve, iris/ciliary body, and choroid (E) and the tissue-specificity of long-lived and short-lived macrophages among eye tissues (F). Statistics were calculated using Two-way ANOVA with Bonferroni's post-hoc test.

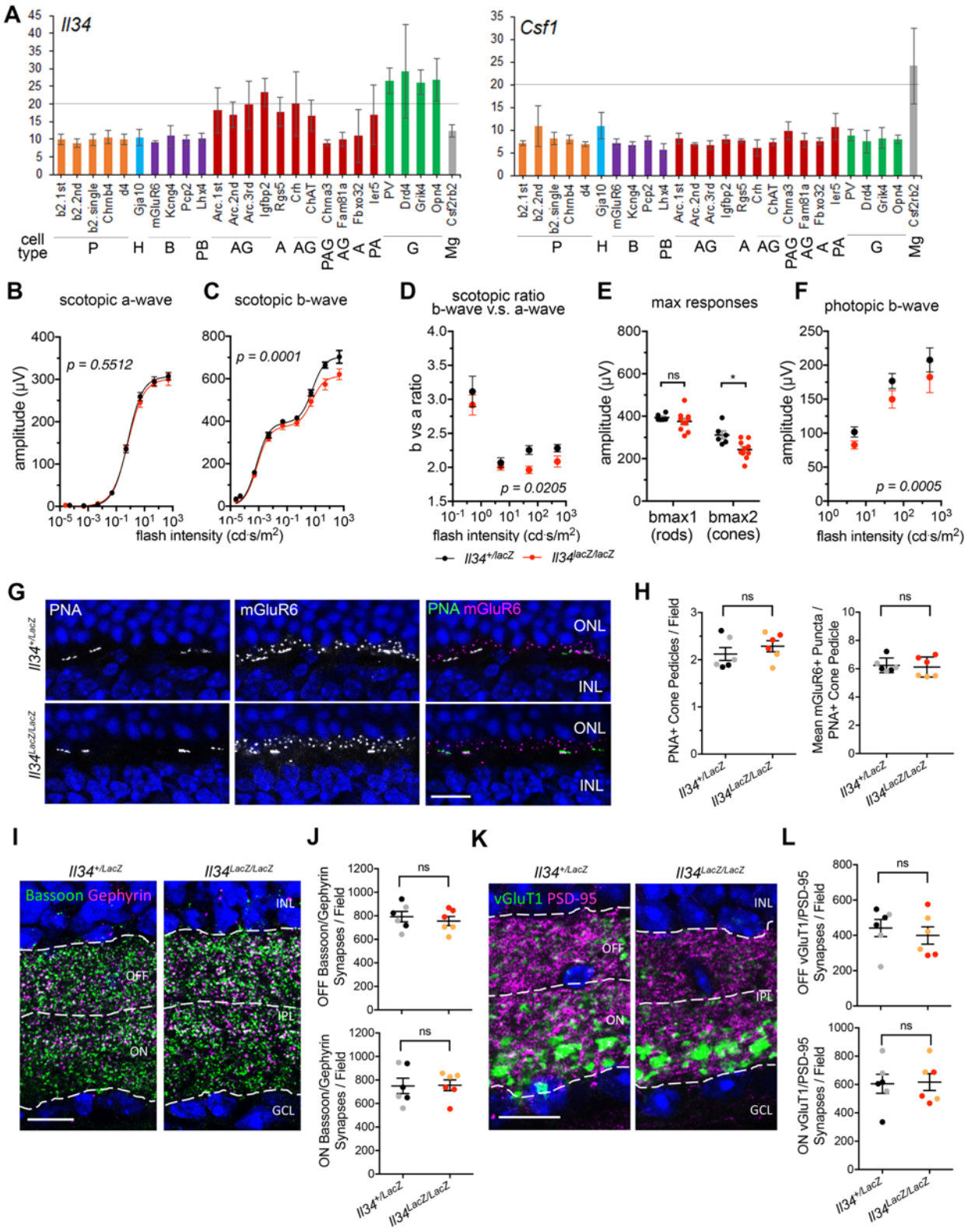
A
Il34
Csf1
cell type
P
H
B
PB
AG
A
AG
PAG
AG
A
PA
G
Mg
B
scotopic a-wave
p = 0.5512
amplitude (μV)
flash intensity (cd·s/m²)
C
scotopic b-wave
p = 0.0001
D
scotopic ratio
b-wave v.s. a-wave
b vs a ratio
p = 0.0205
flash intensity (cd·s/m²)
Il34+/lacZ
Il34lacZ/lacZ
E
max responses
amplitude (μV)
ns
*
bmax1 (rods)
bmax2 (cones)
F
photopic b-wave
amplitude (μV)
p = 0.0005
flash intensity (cd·s/m²)
G
PNA
mGluR6
PNA mGluR6
ONL
INL
Il34+/LacZ
Il34LacZ/LacZ
H
PNA+ Cone Pedicles / Field
Mean mGluR6+ Puncta / PNA+ Cone Pedicle
ns
I
Bassoon Gephyrin
OFF
IPL
ON
INL
GCL
J
OFF Bassoon/Gephyrin Synapses / Field
ON Bassoon/Gephyrin Synapses / Field
K
vGluT1 PSD-95
L
OFF vGluT1/PSD-95 Synapses / Field
ON vGluT1/PSD-95 Synapses / Field

Figure S2. IL-34 Dependent Contributions to Other Light Responses of Retina, Related Figure 2. (A) The expression level of *Il34* and *Csf1* in different retinal cell types using the database (Siegert et al, 2011). P, photoreceptors; H, horizontal cells; B, bipolar cells; A, amacrine cells; G, cells in ganglion layer; Mg, microglia. **(B-F)** Comparisons of scotopic a-wave (B), scotopic b-wave (C), scotopic ratio of b-wave and a-wave (D), max responses of scotopic b-wave (E) and photopic b-wave (F) between $Il34^{+/LacZ}$ and $Il34^{LacZ/LacZ}$ mice. $Il34^{+/LacZ}$, n = 6; $Il34^{LacZ/LacZ}$, n = 10. **(G-L)** Synapse numbers are unchanged in *Il34* mutants. *N* = 2 animals of each genotype. Dots of the same color represent ROIs from the same animal. Data are expressed as mean ± SE. All scale bars, 10 μm. (G) Representative images of cone synapses in the OPL of *Il34* mutants. Peanut agglutinin (PNA) labels cone pedicles; anti-mGluR6 labels postsynaptic sites at tips of ON bipolar cell dendrites. Colocalization reveals cone synapses, and remaining mGluR6+ puncta are rod synapses**.** (H) Quantification of cone pedicles (left) and cone synapses onto ON bipolar cells (right) in *Il34* mutants and heterozygous controls. (I) Representative images of the IPL with inhibitory synapses marked by colocalization of anti-bassoon (presynaptic, green) and anti-gephyrin (postsynaptic, magenta) in *Il34* mutant retinas. OFF and ON regions of the IPL were analyzed separately (dashed lines). (J) Quantification of bassoon/gephyrin synaptic puncta in OFF (top) and ON (bottom) IPL sublaminae. (K) Representative images of the IPL with excitatory synapses marked by colocalization of anti-vGluT1 (presynaptic, green) and anti-PSD-95 (postsynaptic, magenta) in *Il34* heterozygous and homozygous adult mouse retinas. OFF and ON regions of the IPL were analyzed separately (dashed lines). (L) Quantification of vGluT1/PSD-95 synaptic puncta in the OFF (top) and ON (bottom) IPL sublaminae.

Figure S3

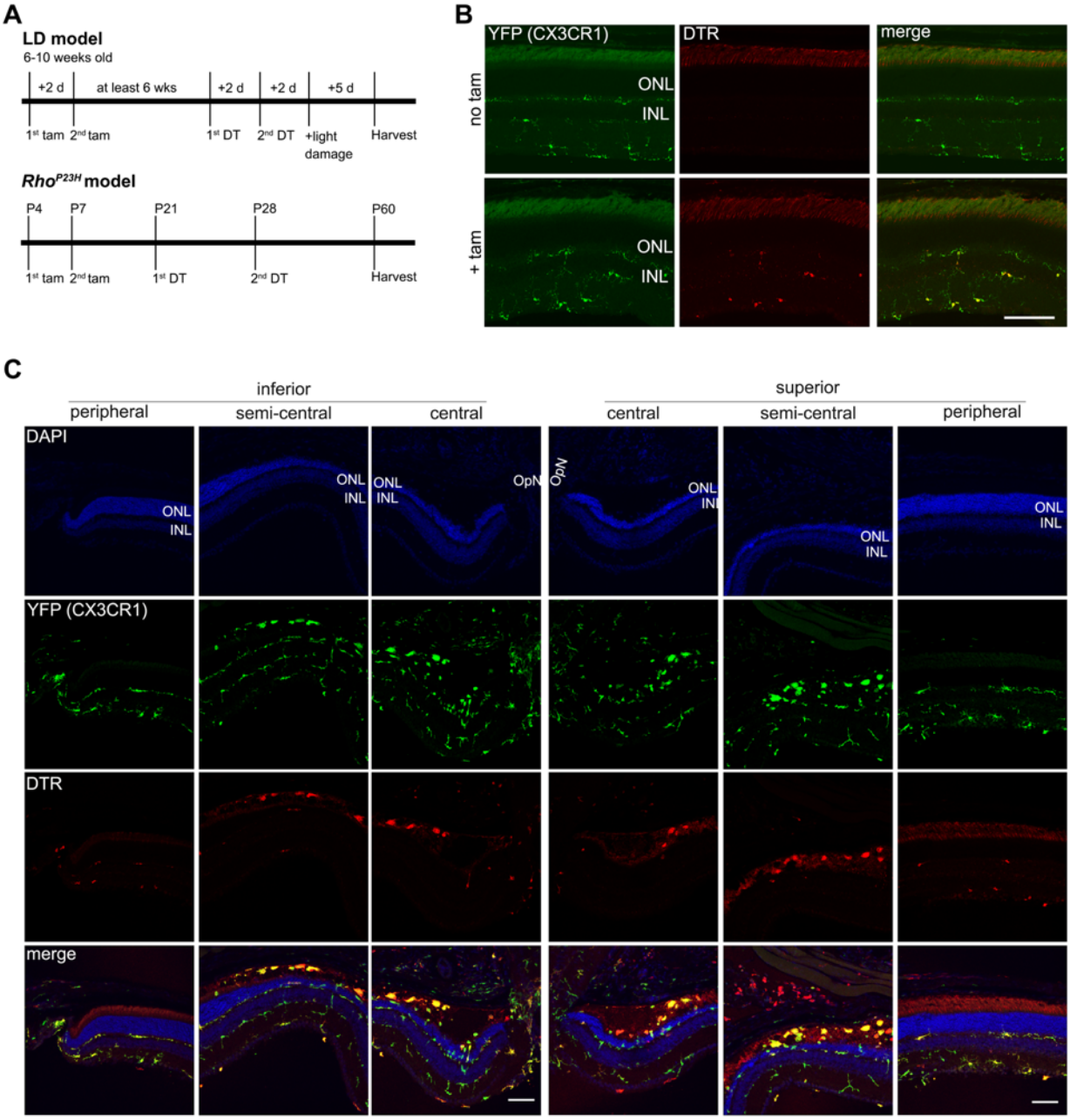

Figure S3. Depletion of srMG in LD Model and *Rho*^{P23H} model, Related to Figure 3. (A) Schematic flow of microglia depletion in LD model (top) and *Rho*^{P23H} mice (bottom). **(B)** Representative images show DTR+ microglia (Cx3cr1^{YFP}, green; DTR, red) in lineage tracing of F1-iDTR mice. Mice not receiving tam were used as controls. Scale bars, 100 μm. **(C)** Representative images of retinal cross sections from different regions of the same mouse show the asymmetric distribution of subretinal niche microglia (DAPI, blue; YFP, green; DTR, red)

between inferior and superior regions in F1-iDTR mice under the LD setting. Scale bars, 100 μm.

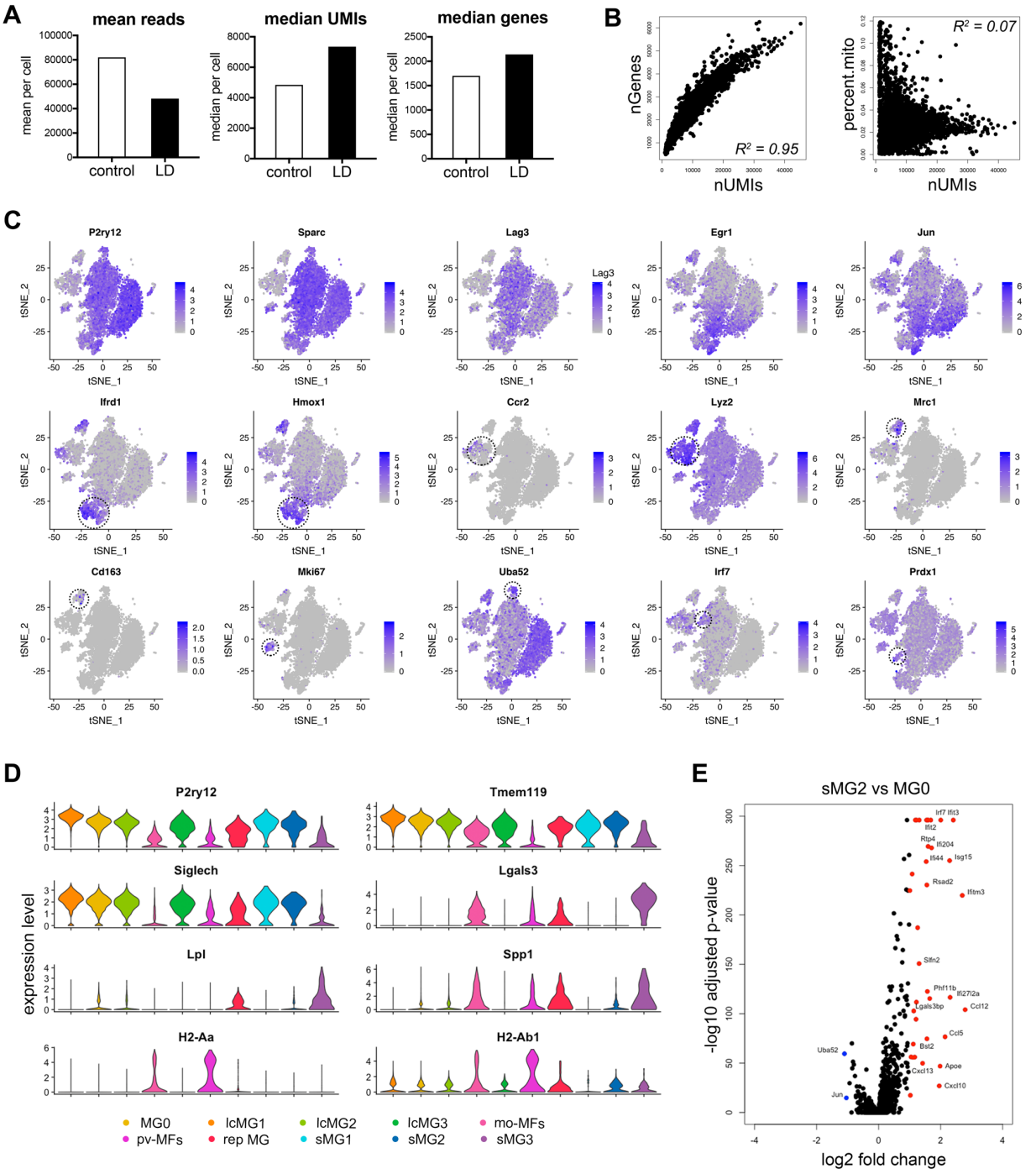

Figure S4. Single Cell RNA-Seq Clusters in Retinal Degeneration, Related to Figure 4. (A) Parameters of single cell RNA-seq from Cell Rangers were shown. **(B)** Correlations between the number of UMIs and the number of genes per cell or mitochondria gene percentage were evaluated using Seurat with Pearson's Correlation (R^2). **(C)** Marker genes in Fig 4B were shown using FeaturePlot() of Seurat. **(D)** Violin plots depict expression changes of marker genes as

indicated across ten major clusters described in (Fig 4A) on the x axis. **(E)** Volcano plot shows the fold change of genes (x axis, log2 scale) and significance (y axis, -log10 scale) between sMG2 to homeostatic microglia (MG0).

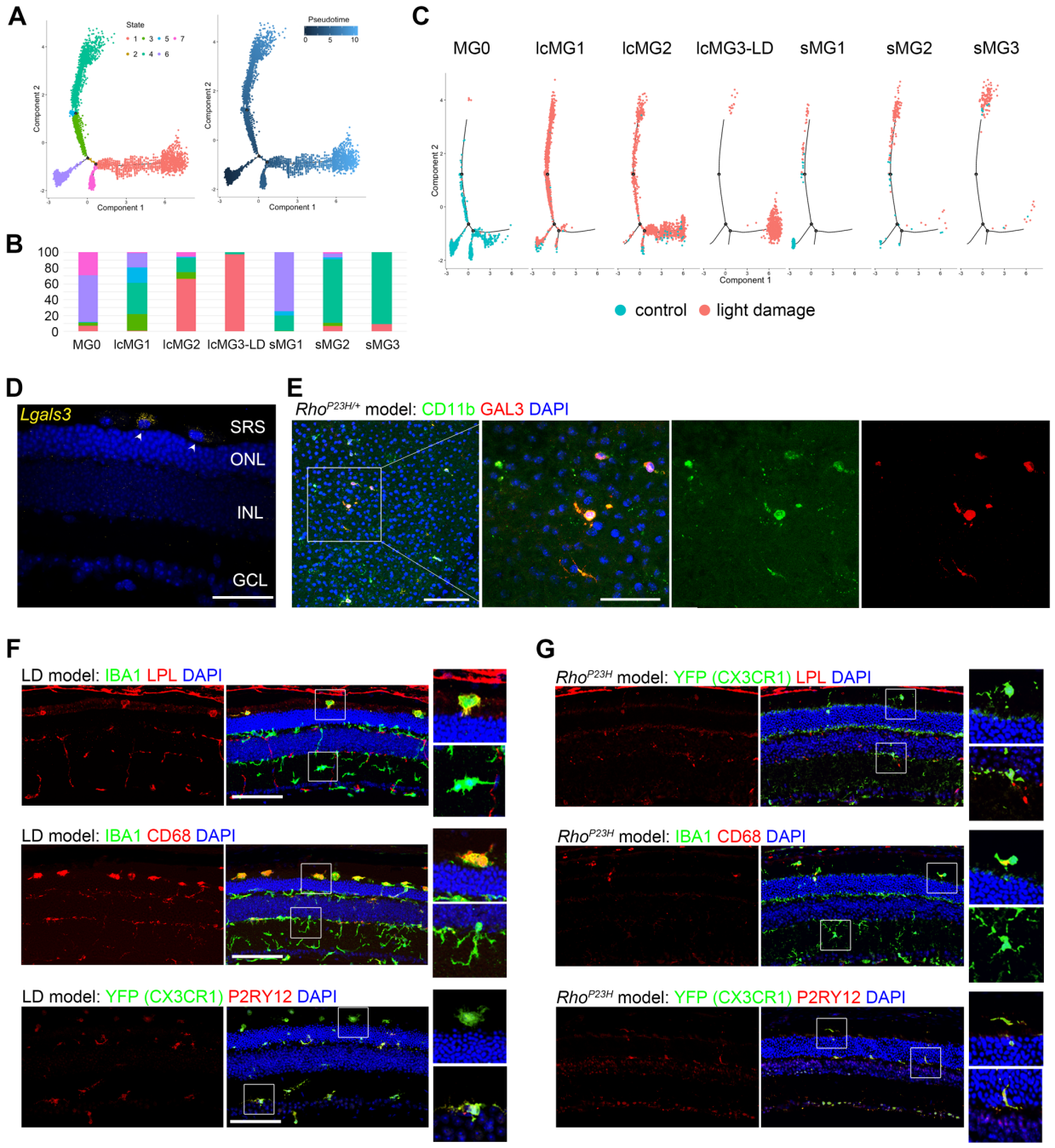

Figure S5. Identification and Validation of srMG Markers, Related to Figure 5. (A) Trajectory plots suggest seven states of retinal microglia upon LD. MG0 was set as the initial state with pseudotime = 0. **(B)** The % of states in each cluster is shown. **(C)** Dot plots show cell distribution along the trajectory of each cluster from control and light damage as indicated. **(D)** RNAScope *in situ* hybridization of *Lgals3* in LD model. **(E)** Representative images show GAL3^{+} (red) subretinal microglia in RPE flat mounts (D) of *Rho*^{P23} mice (IBA1 or CD11b, green). Scale bar, 100 μm. **(F,G)** Immunostaining of LPL, CD68, P2RY12 (all in red) and IBA1 or YFP (green)

in the retinal cross sections shows the localization of sMG3 in the SRS of LD model (F) and two-month old *Rho*^{P23H} mice (G). Images (D-G) were acquired from 3 to 6 mice in three independent experiments. See Table S2 for details. Scale bars, 100 μm.

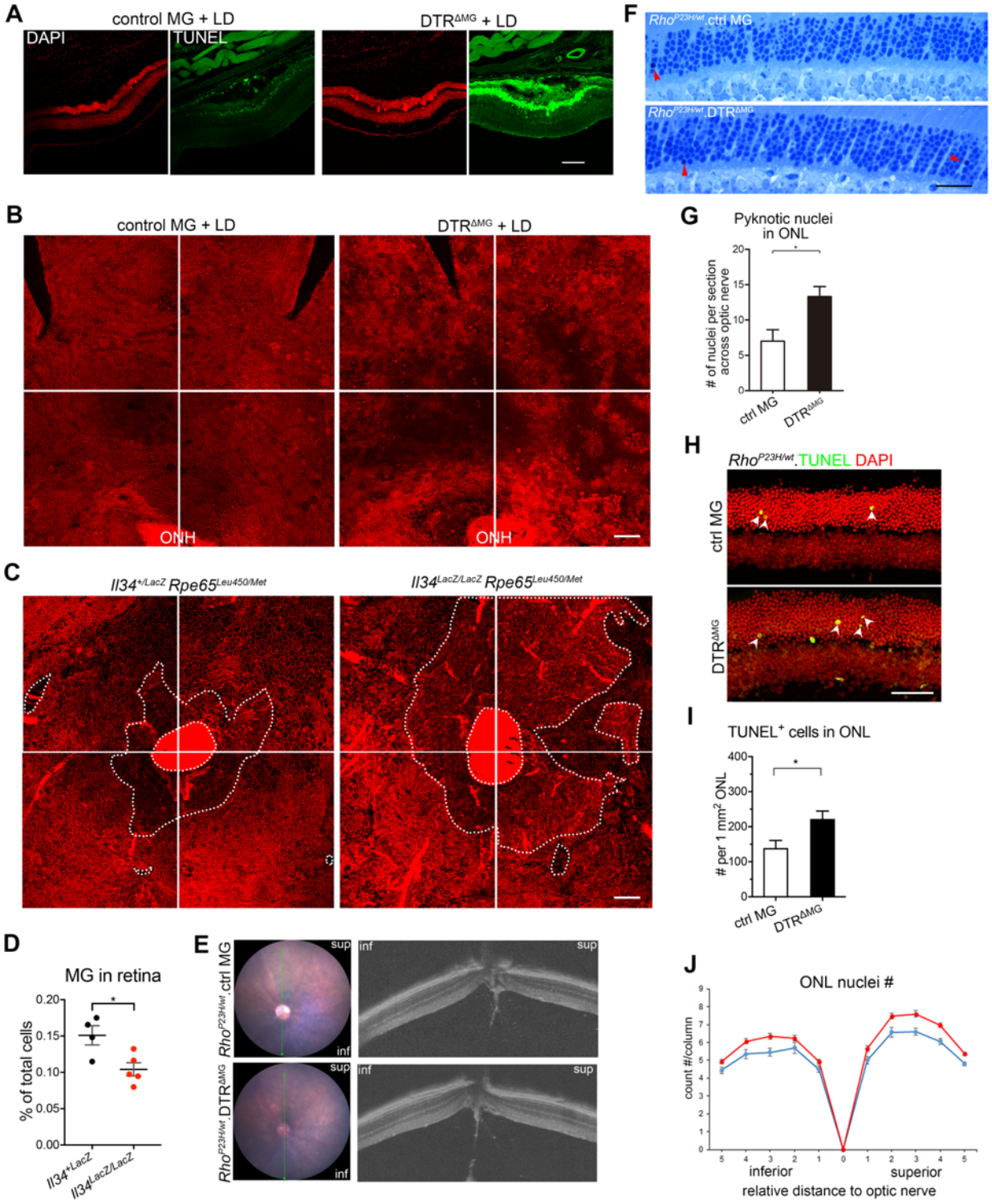

Figure S6. Characterization of Photoreceptor Degeneration in Microglia Depletion Settings, Related to Figure 6. (A) Representative images of retinal cross sections show abundant TUNEL^{+} staining (green) in DTR$^{\Delta MG}$ retina upon LD. DAPI, red. Scale bar, 100 μm. **(B, C)** Representative images from stitched fields of the RPE in CBF1 (B) and *Il34^{LacZ}*

Rpe65$^{Leu450/met450}$ mice (C) under LD settings. Scale bars, 100 μm. **(D)** Dot plots (mean ± SEM) depict the % of microglia compared to total viable singlets in retina using flow cytometry between *Il34*$^{+/LacZ}$ and *Il34*$^{LacZ/LacZ}$ mice. Each dot represents one mouse. **(E)** Fundus imaging (left) and OCT (right) show no obvious morphological alteration in *Rho23*^{P23H} mice. **(F)** Representative images compare pyknotic nuclei in ONL as indicated by red arrow heads between *Rho23*^{P23H}.control MG and DTR$^{\Delta MG}$ mice. Scale bar, 100 μm. **(G)** Bar graphs (mean ± SEM) summarize the number of pyknotic nuclei in ONL shown in (F). *Rho23*^{P23H}.control MG mice, n = 4; *Rho23*^{P23H}.DTR$^{\Delta MG}$ mice, n = 10. **(H)** TUNEL staining (green) in the retinas of *Rho23*^{P23H} mice with/without microglia depletion. DAPI, red. Scale bar, 100 μm. **(I)** Bar graphs (mean ± SEM) summarize the number of TUNEL^{+} cells in ONL shown in (H). N = 5 mice per group. **(J)** Quantification of the outer nuclear layer shows the increased cell number in the *Rho23*^{P23H}.DTR$^{\Delta MG}$ mice. *Rho23*^{P23H}.control MG mice, n = 10; *Rho23*^{P23H}.DTR$^{\Delta MG}$ mice, n = 15.

Table S1. List of Marker Genes in the Cluster Heatmap, Related to Figure 4

Genes	Cluster ID	Genes	Cluster ID
Uba52	MG0_1	H2-Eb1	mo-MFs_5
Ier5	MG0_1	Gpnmb	mo-MFs_5
P2ry12	MG0_1	Fabp5	mo-MFs_5
Gm10073	MG0_1	Cxcl2	pv-MFs_6
Gpr34	MG0_1	Cxcl1	pv-MFs_6
P2ry13	MG0_1	Il1b	pv-MFs_6
Rhob	MG0_1	Ccl7	pv-MFs_6
Gm26825	MG0_1	Phlda1	pv-MFs_6
Jun	MG0_1	Ccl2	pv-MFs_6
Gm26522	MG0_1	Stmn1	repMG_7
Sparc	lcMG1_2	Hmgb2	rep MG_7
Man2b1	lcMG1_2	2810417H13Rik	rep MG_7
Lag3	lcMG1_2	Top2a	rep MG_7
Cox7a2l	lcMG1_2	Birc5	rep MG_7
Lgals3bp	lcMG1_2	Tuba1b	rep MG_7
Ifi27l2a	lcMG1_2	H2afz	rep MG_7
Zfos1	lcMG1_2	Tubb5	rep MG_7
Eef1b2	lcMG1_2	Smc4	rep MG_7
Itgam	lcMG1_2	Ube2c	rep MG_7
Ppfia4	lcMG1_2	Rpl23a-ps3	sMG1_8
Egr1	lcMG2_3	Gm10076	sMG1_8
Nfkbia	lcMG2_3	Rps18-ps3	sMG1_8
Fos	lcMG2_3	Rpl9-ps6	sMG1_8
Junb	lcMG2_3	Rpl6l	sMG1_8
Ier2	lcMG2_3	Grcc10	sMG1_8
Btg2	lcMG2_3	RP23-81F19.2	sMG1_8
Ccrl2	lcMG2_3	Syngr1	sMG1_8
Zfp36	lcMG2_3	Ifit3	sMG2_9
Hspa1b	lcMG2_3	Phf11b	sMG2_9
Ifrd1	lcMG3_4	Ifit2	sMG2_9
Hmox1	lcMG3_4	Ifit3b	sMG2_9
Il1a	lcMG3_4	Usp18	sMG2_9
Tnf	lcMG3_4	Isg15	sMG2_9
Cd83	lcMG3_4	Ifit1	sMG2_9
Atf3	lcMG3_4	Ccl12	sMG2_9
Kdm6b	lcMG3_4	Irf7	sMG2_9
Icam1	lcMG3_4	Cxcl10	sMG2_9
Ccl4	lcMG3_4	Lgals3	sMG3_10
Ccl3	lcMG3_4	Prdx1	sMG3_10
Lyz2	mo-MFs_5	Plin2	sMG3_10
Ms4a7	mo-MFs_5	Vim	sMG3_10
Ms4a6c	mo-MFs_5	Lilrb4a	sMG3_10
H2-Ab1	mo-MFs_5	Lilr4b	sMG3_10
Cd74	mo-MFs_5	Sqstm	sMG3_10
Spp1	mo-MFs_5	Mmp12	sMG3_10
H2-Aa	mo-MFs_5		

Table S2. Summary Data of Immunostaining/RNAScope Validation of sMG3 Markers

Marker (Method)	Model	# of mice	sex	# of mice with positive markers
Gals3(antibody)/ *Lgals3* (RNAScope)	LD	6	♂, 4; ♀, 2	All
Cd68 (antibody)	LD	4	♂, 2; ♀, 2	All
Lpl (antibody)	LD	4	♂, 2; ♀, 2	All
Gals3(antibody)	*Rho*^{P23H}	4	♂, 3; ♀, 1	All
Cd68 (antibody)	*Rho*^{P23H}	3	♂, 2; ♀, 1	All
Lpl (antibody)	*Rho*^{P23H}	3	♂, 2; ♀, 1	None